A Transparent, Self-Healing, Highly Stretchable Ionic Conductor

Yue Cao, Timothy G. Morrissey, Eric Acome, Sarah I. Allec, Bryan M. Wong, Christoph Keplinger, and Chao Wang**

Self-healing refers to the ability of a material to heal itself upon mechanical damage. Nature has perfected mechanisms of self-healing through evolution into a preeminent survival feature of biological systems.[1–3] Similarly, man-made materials with self-healing capabilities are highly desirable for areas of application spanning from weather resistant surfaces to robust electronics.[4–16] The ability to rationally tune and add new functionality in materials can lead to transformative advances in emerging self-healing systems. Recent discoveries include self-healing conductors,[17,18] self-healing superhydrophobic surfaces,[9,19] and self-healing sensors.[20–22] Inspired by wound healing in nature, functional self-healing materials repair damage caused by wear and thus extend lifetime and lower cost of materials and devices. A wide range of devices can benefit from the integration of self-healing capabilities, such as high-performance electronic skin,[23] lithium ion batteries with greatly improved lifetime,[24] self-healing supercapacitors based on a self-healing polymer composite,[25] and self-healing heat sensors.[21]

Ionic conductors are a class of functional materials with key roles in energy storage,[26–28] solar energy conversion,[29] sensors,[22,30,31] and electronic devices.[32–36] In particular, hydrogels containing electrolytes offer a unique combination of high stretchability, transparency, and biocompatibility. They show great promise in stretchable ionic devices, such as electrically activated, soft, transparent actuators and loudspeakers[37] and ionic skins that can sense the location and pressure of touch.[30,31] Hydrogels containing deliquescent salts retain water in environments with low relative humidity,[38] and ionogels are nonvolatile even in vacuum.[39] Transparent, electrically activated artificial muscles[37] are stretchable ionic devices based on the layered structures of dielectric elastomers and stretchable ionic conductors. Each layer is subject to considerable mechanical and electrical stresses, and the integration of self-healing capabilities promises to substantially improve reliability. While we have already seen successful demonstrations of artificial muscles with self-healing, nontransparent dielectric layers,[40] and while others have demonstrated self-healing gels[41–43] with one or two functional properties, the development of an ionic conductor that is simultaneously transparent, mechanically stretchable, and features self-healing, remains a considerable challenge. The key difficulty in the design of a self-healing ionic conductor is the identification of bonds that are stable and reversible under electrochemical conditions. Conventionally, self-healing polymers make use of noncovalent bonds, such as hydrogen bonds,[7,8] metal–ligand coordination bonds,[44] and dynamic covalent bonds,[6,14] and are easily affected by electrochemical reactions that degrade the mechanical performance of these materials. Ionomers, a commercially available self-healing polymer,[45] require an external stimulus such as temperature to increase polymer chain mobility and activate self-healing.[46,47]

Herein, we introduce a transparent, highly stretchable ionic conductor with autonomous self-healing capability by harnessing ion–dipole interactions as the dynamic bonds for self-healing. This material tolerates extreme strains exceeding 5000%, features an ionic conductivity of 10^{-4} S cm^{-1}, and shows high transparency across the visible spectrum with an average transmittance of 92%. More importantly, the material can completely heal mechanical properties within 24 h at room temperature without any external stimulus. We illustrate the unique combination of attractive properties of the transparent, self-healing, highly stretchable ionic conductor when used to electrically activate transparent artificial muscles that autonomously heal after severe mechanical damage.

The basic idea in the design of this polymeric material is to use a polar, stretchable polymer combined with a mobile, high-ionic-strength salt. Thus, the polymer chains are cross-linked by ion–dipole interactions between the polar groups on the polymer and the ionic salt. Ion–dipole interactions are forces between charged ions and polar molecules. The strength of the bond increases as ion charge or molecular polarity increases. Examples of ion–dipole interactions between ionic liquids

Dr. Y. Cao, Prof. C. Wang
Department of Chemistry
University of California
Riverside, CA 92521, USA
E-mail: chaowang@ucr.edu, wangc@scut.edu.cn
T. G. Morrissey, E. Acome, Prof. C. Keplinger
Department of Mechanical Engineering
University of Colorado
Boulder, CO 80309, USA
E-mail: Christoph.Keplinger@colorado.edu
S. I. Allec, Prof. B. M. Wong
Department of Chemical & Environmental Engineering
and Materials Science & Engineering Program
University of California
Riverside, CA 92521, USA
Prof. C. Keplinger
Materials Science and Engineering Program
University of Colorado
Boulder, CO 80309, USA
Prof. C. Wang
Institute of Polymer Optoelectronic Materials and Devices
State Key Laboratory of Luminescent Materials and Devices
South China University of Technology
Guangzhou 510640, P. R. China

DOI: 10.1002/adma.201605099

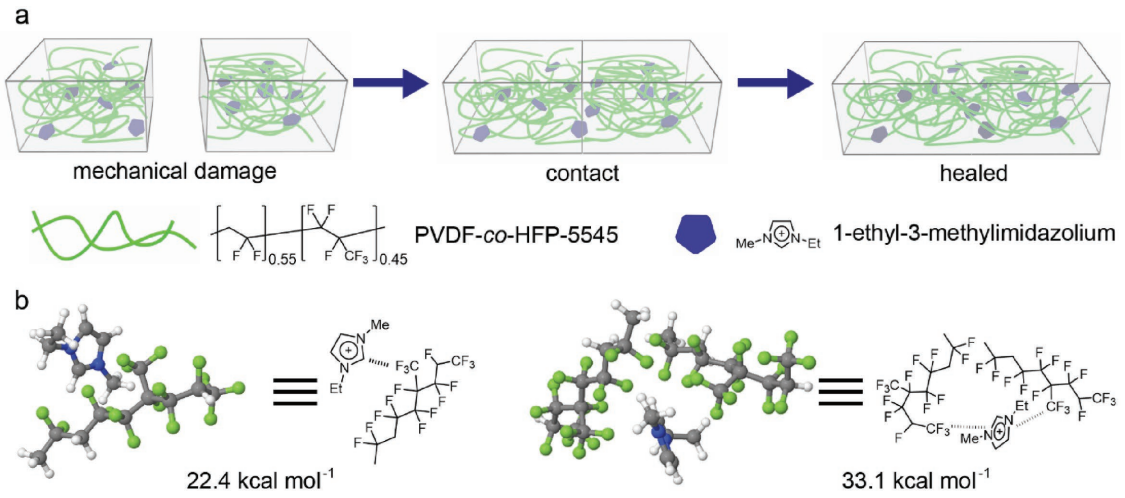

Scheme 1. Design concept for a transparent, self-healing, highly stretchable ionic conductor using ion–dipole interaction as the dynamic motif. a) Demonstration of healing process and chemical structure of polymer and imidazolium cation. Counter anion trifluoromethanesulfonate was omitted for simplicity. b) DFT-optimized structure of imidazolium cation interacting with one or two PVDF-*co*-HFP-5545 monomers. All DFT calculations were carried at the ωB97X-D/6-31G(d,p) level of theory.

and fluorinated polymers are present in various systems.[48–51] Importantly, ion–dipole interactions are highly stable even under electrochemical conditions, which has been proven with a number of gel electrolytes.[52–56] Moreover, the material introduced here differs from traditional ion gels because it has a relatively low content of ionic liquid, a low level of leakage of ionic liquid out of the material, and unique mechanical properties (see Section "Comparison with typical ion gels" of the Supporting Information).

To make the self-healing ionic conductors, we chose poly(vinylidene fluoride-*co*-hexafluoropropylene) (PVDF-*co*-HFP) as the polar polymer network. As shown in **Scheme 1**, the polymer contains two building units, VDF (which is crystalline and less polar) and HFP (which is amorphous and highly polar). Conventional PVDF-*co*-HFP copolymers have VDF ratios larger than 85 mol% and are highly crystalline with a dipole moment of around 2.5 Debye. In comparison, our elastic PVDF-*co*-HFP (PVDF-*co*-HFP-5545) polymer contains a much higher HFP component of 45%, leading to a much lower crystallinity and a very high dipole moment of 5.507 Debye.[57] Upon addition of high-ionic-strength ionic liquids into the polymer, there will be two effects: first, the ionic liquid will plasticize the polymer chains to a much lower glass transition temperature below room temperature; second and more importantly, the polymer chains are cross-linked by highly reversible ion–dipole interactions. The combination of these two effects gives the polymer the capability to self-heal autonomously at room temperature.

To gain further insight into the ion–dipole interactions, we carried out several density functional theory (DFT) calculations at the ωB97X-D/6-31G(d,p) level of theory. The ωB97X-D functional was specifically chosen due to its accurate description of both dispersion forces and thermochemistry for both neutral and ionic molecules.[58,59] Molar ratios of dipole (CF_3) to ion (imidazolium) of 1:1 and 2:1 were chosen for DFT calculations since these values bracket common experimental values. We used oligomer (n = 2) of PVDF-*co*-HFP-5545 to explore the interactions between the polymer and the imidazolium cation. We performed a full geometry optimization of a single oligomer of PVDF-*co*-HFP-5545 in the presence of one imidazolium cation (Figure S1, Supporting Information) and obtained an attractive binding energy of 22.4 kcal mol^{-1}. The ion–dipole interaction here is nearly twice the binding energy between oligomers, which is 11.3 kcal mol^{-1}. We also carried out calculations of one imidazolium cation proximal to two separate oligomers and obtained a significantly stronger binding energy of 31.1 kcal mol^{-1}. These calculations further verified the enhanced intermolecular stability and the favorable ion–dipole interactions within the self-healing polymers.

In our experimental studies, we chose imidazolium salts as the ionic liquids because of their high ionic strength and good electrochemical stability. Owing to a strong ion–dipole interaction (22.4 kcal mol^{-1}), this type of ionic liquid is firmly held in a PVDF-*co*-HFP-5545 polymer matrix and the complex is highly stable over time. The strong interaction of the ionic liquid with the polymer prevents leakage out of the material, a process that is commonly observed in other types of ionic conductors[60] and that can negatively affect the lifetime of devices. Also, we found that counter ions play an important role in the properties of the ionic conductor (see Section "Selection of ionic liquids" and Figures S2–S4 of the Supporting Information). With 1-butyl-3-methylimidazolium chloride (BMICl), the two materials were not compatible, and we failed to obtain a well-mixed sample, likely due to the strong binding between chloride and imidazolium. With the 1-butyl-3-methyl imidazolium tetrafluoroborate ($BMIBF_4$), the ionic conductor was translucent and phase separation structures could be observed in the composite. We were able to get a transparent, stretchable material only with 1-ethyl-3-methylimidazolium trifluoromethanesulfonate (EMIOTf). Even with an ionic liquid amount of 43 wt% (1.53:1 molar ratio CF_3 to imidazolium), the average transmittance of a 0.01 mm thick polymer film was 92%. The absorption band at 400–500 nm is due to the absorption of the ionic liquid (**Figure 1**a and Figure S5 (Supporting Information)). As indicated by the scanning electron microscope (SEM) (Figure 1b)

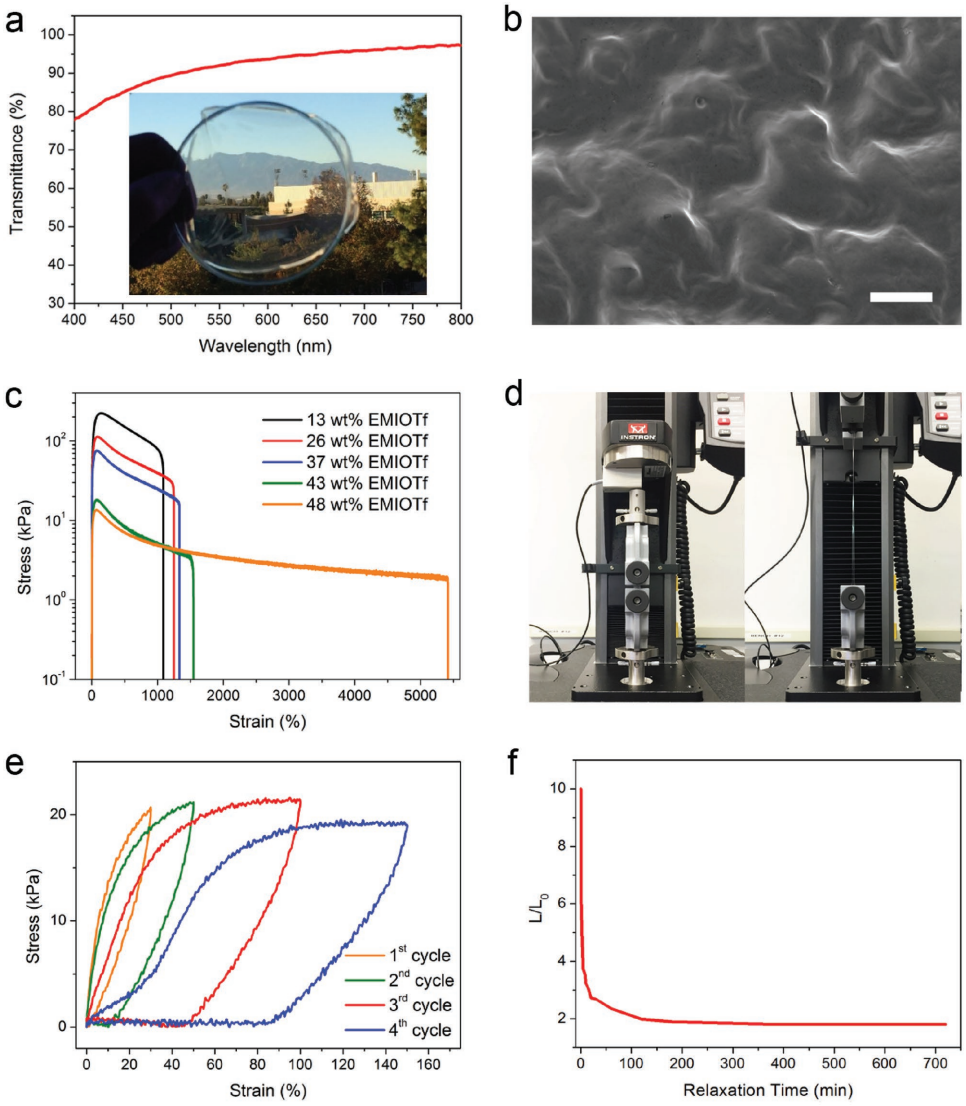

Figure 1. Physical and mechanical properties of the PVDF-*co*-HFP-5545/EMIOTf materials. a) Transmittance spectrum of 43 wt% EMIOTf with a film thickness of 0.01 mm. Inset: Photo of the film on a glass petri dish. b) SEM image of 43 wt% EMIOTf. Scale bar, 10 µm. c) Tensile strain tests of the polymer materials with different amounts of ionic liquid. Maximum strain exceeded 5000% for the sample with 48 wt% EMIOTf. d) Photos illustrating the extreme stretchability of 48 wt% EMIOTf. Left: Pristine 48 wt% EMIOTf sample with a length of 5 mm. Right: 48 wt% EMIOTf stretched to 30 times its initial length. e) Stress–strain cycling tests of 43 wt% EMIOTf. 43 wt% EMIOTf showed elastic behavior up to 50% strain. f) A tensile set test of pristine 43 wt% EMIOTf. After being stretched to ten times its original length, 43 wt% EMIOTf returned back to two times its original length in 2 h.

and X-ray diffraction data (Figure S6, Supporting Information), a continuous homogenous phase indicated good miscibility of ionic liquid and polymer without any microphase segregation.

By tuning the weight ratio of polymer and ionic liquid (EMIOTf), a series of polymer materials with distinct mechanical properties were obtained. As shown in Figure 1c, when increasing the content of ionic liquid up to 48 wt%, (1.23:1 molar ratio CF_3 to imidazolium), the material had a higher stretchability, lower Young's modulus, and lower maximum tensile stress. However, a further increase of the content of ionic liquid to 58 wt% EMIOTf decreased the stretchability of the material (Figure S7, Supporting Information). The 43 wt% EMIOTf polymer material exhibited a Young's modulus of 0.1 MPa, which is comparable to conventional soft rubbers. All material compositions showed good stretchability, in which 48 wt% EMIOTf showed the highest stretchability with strains exceeding 5000% (Figure 1d). The polymers exhibited fully reversible behavior for strains below 50% and returned back to their original length immediately (Figure 1e). At higher strains, the polymers were not fully reversible. However, even being stretched to ten times its original length, the polymer could gradually return back to two times its original length within 2 h (Figure 1f). It is also noteworthy that the polymer possessed a larger modulus at higher loading rates (Figure S8, Supporting Information) and also exhibited creep behavior under constant engineering stress (Figure S9, Supporting Information); both observations are typical for supramolecular rubbery materials.[61,7]

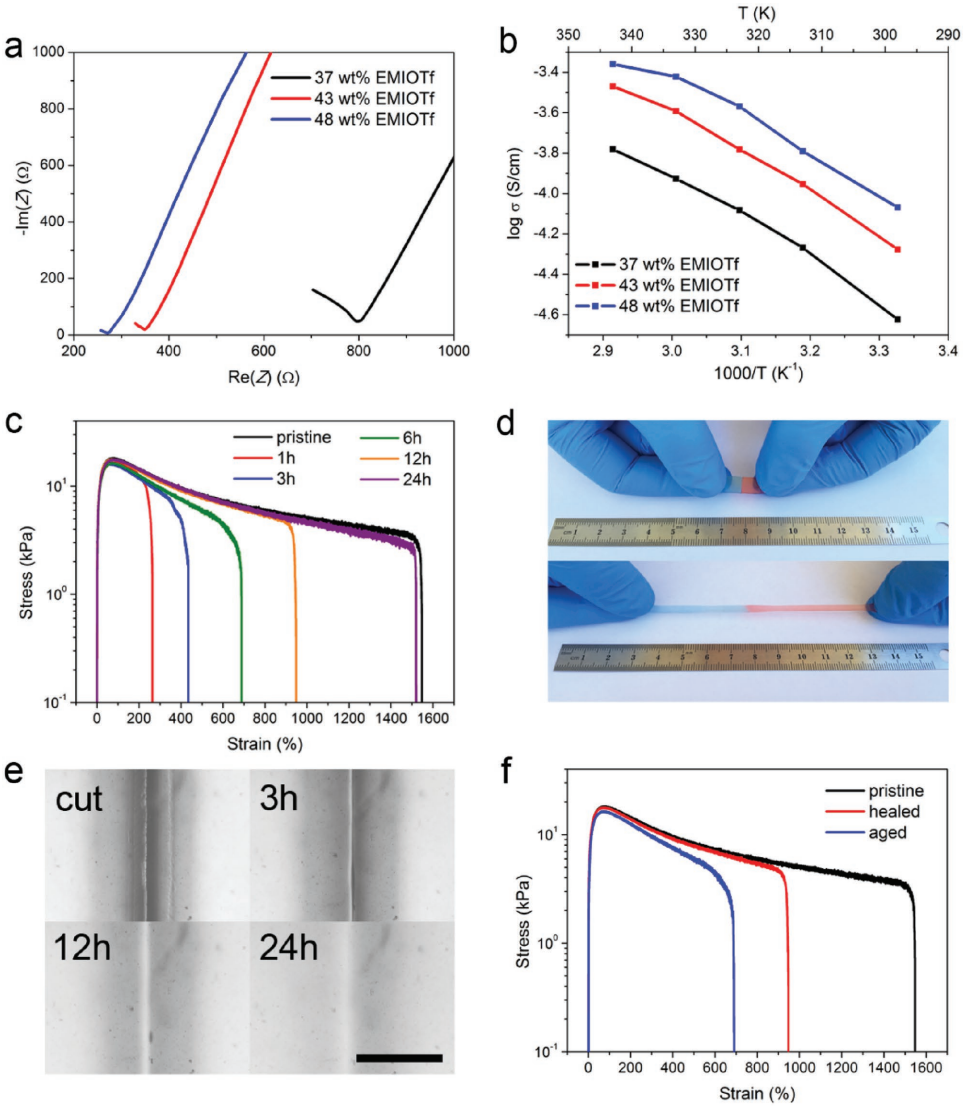

Figure 2. Ionic conductivity and self-healing properties of PVDF-*co*-HFP-5545/EMIOTf materials. a) Impedance plot of 37, 43, and 48 wt% EMIOTf at 25 °C. The samples were 2 cm^2 in area with a thickness of 0.2 mm. b) Temperature dependence of the ionic conductivities of 37, 43, and 48 wt% EMIOTf in the temperature range from 25 to 70 °C. c) Typical stress–strain curves of pristine and healed samples for different healing times at room temperature for 43 wt% EMIOTf. d) Photos of a healed 43 wt% EMIOTf sample in the undeformed state and stretched to five times its original length. e) Optical microscope images of a cut 43 wt% EMIOTf sample after different healing times at room temperature. The damaged sample fully healed after 24 h. Scale bar, 500 µm. f) Typical stress–strain curves for 43 wt% EMIOTf: (i) a pristine sample, (ii) a sample that was allowed to heal for 12 h directly after being cut, and (iii) a sample that was cut first, aged in ambient air for 12 h, and then allowed to heal for 12 h at room temperature.

Apart from the high stretchability and high transparency, the polymer material also exhibited high ionic conductivity. **Figure 2**a shows that the ionic conductivities of 37, 43, and 48 wt% EMIOTf at 25 °C were 2.56×10^{-5}, 5.66×10^{-5}, and 7.06×10^{-5} S cm^{-1}, respectively. Figure 2b shows that the dependence of ionic conductivity on temperature from 25 to 70 °C obeyed the Vogel–Tammann–Fulcher relation, which describes the transport of ions in a viscous polymer matrix.[62]

Our highly stretchable ionic conductors showed outstanding self-healing capabilities. After cutting a sample into two completely separate pieces with a razor blade and gently bringing the cut pieces back into contact, the two damaged faces spontaneously self-healed over time under ambient conditions without any external stimulus. We define the mechanical healing efficiency as the proportion of toughness restored relative to the original toughness (area under the stress–strain curve) because this takes into account the restoration of both stress and strain. The healing speeds were monitored by testing mechanical properties at different lengths of healing time (**Table 1**). Take the 43 wt% EMIOTf as an example: the polymer material fully restored all mechanical properties including the Young's modulus, yield strength, and ultimate tensile strain within 24 h (Figure 2c). Notably, after healing for only 5 min, the polymer material could already be stretched to two times its original length. As demonstrated in Figure 2d, the material tolerated a strain of 500% after healing at room temperature

Table 1. Healing efficiency (defined in terms of the recovered fracture toughness) of PVDF-*co*-HFP-5545 with 43 wt% EMIOTf at different temperatures. The average value and standard deviation were determined from nine individual samples. The samples were taken from three different batches, with each batch providing three samples.

Healing time [h]	At room temperature	At 50 °C
1	30.38 ± 1.98%	54.68 ± 3.36%
3	38.91 ± 0.21%	78.57 ± 3.17%
6	55.47 ± 4.73%	100.34 ± 3.83%
12	75.98 ± 1.64%	100.01 ± 3.37%
24	95.35 ± 0.62%	101.70 ± 5.75%

for 6 h. For all samples, the polymer materials maintained their Young's modulus of 0.1 MPa and followed the same tensile stress curves. The healing capabilities were visualized using an optical microscope. The scar at the damaged interface was fully healed after 24 h at room temperature (Figure 2e). When the healing process was accelerated by raising the temperature to 50 °C, it took 6 h for the samples to fully heal (Table 1 and Figure S10 (Supporting Information)). Additionally, a strip of 43 wt% EMIOTf exhibited a nearly instantaneous return to its original resistance after being cut and after the separated pieces were brought back into contact with each other (Figure S11, Supporting Information). We also confirmed that the highly stretchable ionic conductor itself is highly stable over time. When left at room temperature for one month, the polymer kept its shape and mechanical properties. We did not notice any leaking of the ionic liquid. We further observed that the location that experienced mechanical damage showed aging effects. When we put the freshly cut surfaces together, the polymer could heal 73% within 12 h. However, when the cut surfaces were exposed to ambient air for 12 h, the healing efficiency dropped to 53% (Figure 2f). Nevertheless, when holding the temperature at 50 °C for 12 h, we observed full recovery of the mechanical properties of this sample (Figure S12, Supporting Information). The drop in healing efficiency of aged samples is due to the polymer chains at the freshly cut surface reorientating and forming self-complementary bonds over time. When we brought the surfaces that were cut and aged for 72 h, back into contact, they did not self-heal.

We further investigated the healing mechanism and the role of the ion–dipole interactions using Fourier transform infrared spectroscopy (FTIR). For pure PVDF-*co*-HFP-5545 polymer, the bands located at 1396 and 1178 cm^{-1} were assigned to the wagging of CH_2 and antisymmetric stretching of CF_2, respectively (**Figure 3**a).[63] Characteristic vibrational bands of PVDF-*co*-HFP at 833 and 883 cm^{-1} correspond to the amorphous phase of the polymer. We did not observe vibrational bands related to the crystalline phase of PVDF-*co*-HFP, indicating the amorphous nature of the fluoride polymer. In contrast, the common PVDF-*co*-HFP with 10% HFP (PVDF-*co*-HFP-9010) is a crystalline polymer (Figure S13, Supporting Information). The difference in crystallinity of the PVDF-*co*-HFP-5545 polymer is due to the increased content of HFP. Upon addition of EMIOTf, the bands located at 1396 and 1178 cm^{-1} gradually shifted to higher wavenumbers, which clearly indicates the interactions between the polymer and the imidazolium-based ionic liquid (Figure 3b). With the presence of ion–dipole interactions, the strength of the C—F bond is expected to weaken because of the interactions between imidazolium salt and the C—F dipole on the polymers. This is verified by the shifts of the CF_2 antisymmetric stretching band from 1178 to 1209 cm^{-1}. The plasticizing effect can also be observed from FTIR. As shown in Figure 3c, the CH_2 wagging band shifted from 1396 to 1400 cm^{-1}, indicating a weakened interaction between the H atom and the F atom between the polymer chains. Differential scanning calorimetry (DSC) results provided more direct evidence on the plasticizing effect. As shown in Figure 3d, the glass transition temperature of the material was lowered from −26.2 to −55.9 °C upon the addition of 43 wt% EMIOTf. The ion–dipole interaction and the plasticizing effect both contribute to the self-healing property of the materials. As a control experiment, we used the PVDF-*co*-HFP-9010 with 90 mol% of VDF to make the ionic conductor. As shown in Figure 3e,f, with the same weight percentage of ionic liquid, the material based on PVDF-*co*-HFP-9010 exhibited a Young's modulus 100 times higher than that of PVDF-*co*-HFP 5545. Also, the PVDF-*co*-HFP-9010 remained crystalline in the presence of the ionic liquid (Figure S14, Supporting Information). Moreover, regardless of how much ionic liquid was added, the polymer material did not demonstrate any self-healing capability, due to low polarity and lack of ion–dipole interactions (Figure S15, Supporting Information). These results indicate that the ion–dipole interactions play an important role for the self-healing capabilities.

We next demonstrated the benefits of self-healing ionic conductors as components of soft machines, a class of devices[64–67] that is receiving increasing interest from both academia and industry. Therefore, we analyzed the performance of two types of stretchable, transparent, ionic conductors when used to electrically activate dielectric elastomer actuators (DEAs).[37,68,69] We compared actuation of DEAs before and after inflicting mechanical damage and when the actuators were activated with (i) an ionogel[38] and (ii) the transparent, self-healing, stretchable ionic conductor introduced in this paper. **Figure 4**a shows a schematic of a circular DEA, based on a layer of dielectric elastomer sandwiched between two stretchable conductors. When high voltage is applied, the oppositely charged conductors exert electrostatic stress on the dielectric elastomer, causing it to compress in thickness and expand in area. In our experiments, we used a dielectric elastomer (VHB 4910, 3M) prestretched biaxially by a factor of 3 and attached to a rigid frame.

Figure 4b (top-left) shows a DEA using ionogel as the stretchable conductor in a pristine condition with voltage off. We actuated the pristine DEA by applying 5 kV across the dielectric (0.11 mm thick after prestretching) and allowed the viscoelastic expansion of the active area of the device to stabilize for 10 s (Figure 4b, top-right). To simulate severe mechanical damage, we then used scissors to cut one circular ionogel layer in half (Figure 4b, bottom-left). The cut pieces of ionogel were brought back to their original locations on the actuator with the cut surfaces in contact with each other. The ionogel layer was allowed to rest for 24 h but remained damaged (Figure 4b, bottom-center). When the DEA with the damaged layer of ionogel was actuated with 5 kV, the cut pieces further separated, leading to nonuniformity and a lower amount of actuation (119.5% area strain) compared to the pristine state (135.4% area strain)

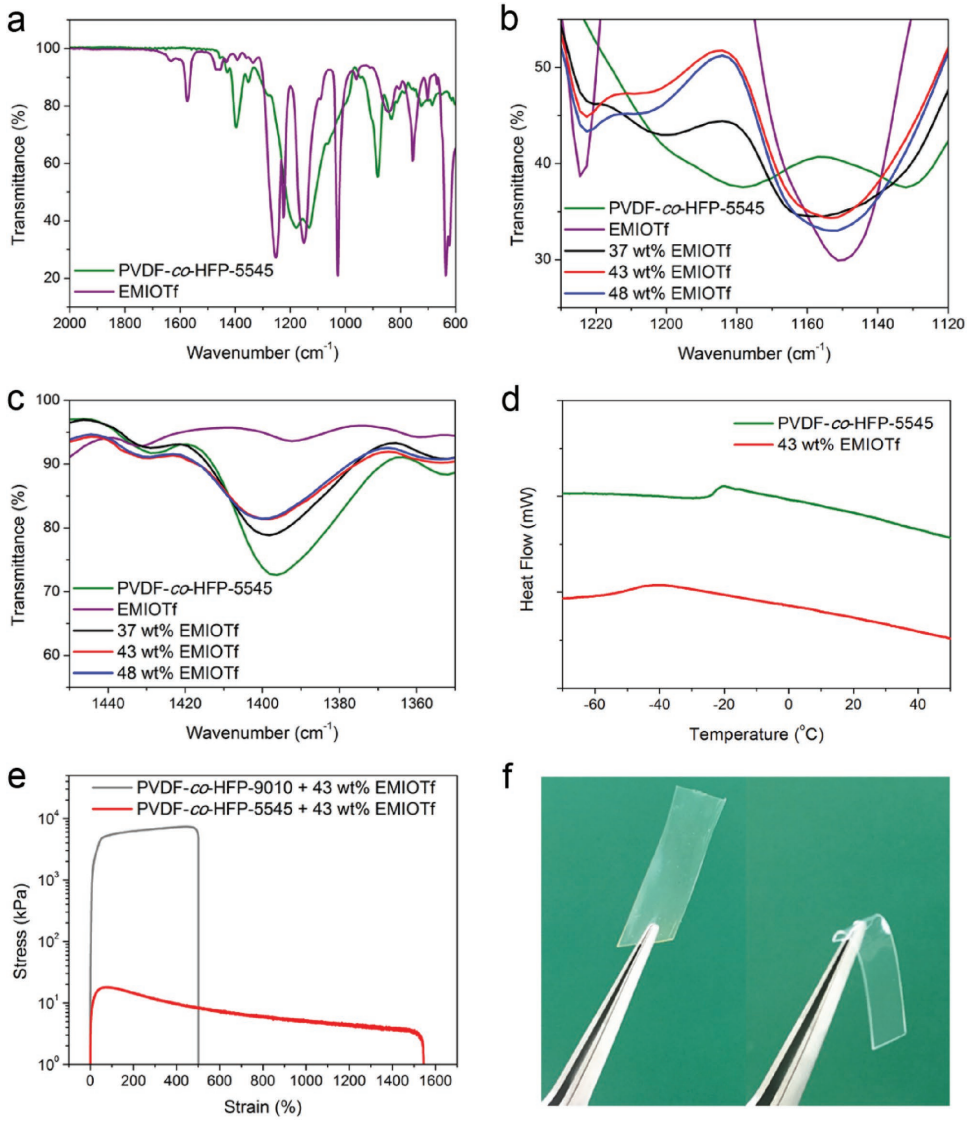

Figure 3. a) FTIR spectrum of PVDF-*co*-HFP-5545 and EMIOTf. 1450–1350 and 1230–1120 cm^{-1} were chosen for detail analysis owing to the weak signals from EMIOTf at these ranges. FTIR spectrum of PVDF-*co*-HFP-5545, EMIOTf, 37 wt% EMIOTf, 43 wt% EMIOTf, and 48 wt% EMIOTf at range from b) 1230–1120 cm^{-1} and c) 1450–1350 cm^{-1}. d) DSC traces of the PVDF-*co*-HFP-5545 and 43 wt% EMIOTf. e) Tensile strain tests of common PVDF-*co*-HFP-9010 with 43 wt% EMIOTf and PVDF-*co*-HFP-5545 with 43 wt% EMIOTf. The Young's modulus of common PVDF-*co*-HFP-9010 with 43 wt% EMIOTf is 9.54 MPa, which is 100 times higher than that of 43 wt% EMIOTf. f) Photos of common PVDF-*co*-HFP-9010 with 43 wt% EMIOTf (left) and PVDF-*co*-HFP-5545 with 43 wt% EMIOTf (right).

(Figure 4b, bottom-right). Additionally, we observed delamination of the ionogel pieces from the dielectric. Video S1 (Supporting Information) visualizes the performance of the DEA with ionogel conductors, depicted in Figure 4b, and shows the damaged ionogel delaminating from the DEA.

We repeated the same experimental steps for a DEA using the transparent, self-healing, highly stretchable ionic conductor. Figure 4c (top-left) shows the actuator in the pristine condition with voltage off. We again actuated the pristine device by applying 5 kV (Figure 4c, top-right). The actuation performance was comparable to that of the pristine actuator using the ionogel. We then used scissors to cut one layer of self-healing ionic conductor in half and placed the cut surfaces in contact with each other (Figure 4c, bottom-left). After 24 h, the cut healed with minimal scarring (Figure 4c, bottom-center). After healing, the DEA was actuated with 5 kV and performed as well as in its pristine state, with uniform actuation, a similar level of area expansion (pristine: 122.6% area strain; healed: 123.5% area strain) and without noticeable separation of the scarred region (Figure 4c, bottom-right). Video S2 (Supporting Information) visualizes the performance of the DEA with self-healing ionic conductors depicted in Figure 4c. Additionally, when we used the self-healing ionic conductor to activate DEAs, we did not observe the dielectric strength of the dielectric layer to be a function of storage time after assembly of the actuator. Therefore, the use of this ionic conductor, which features a low

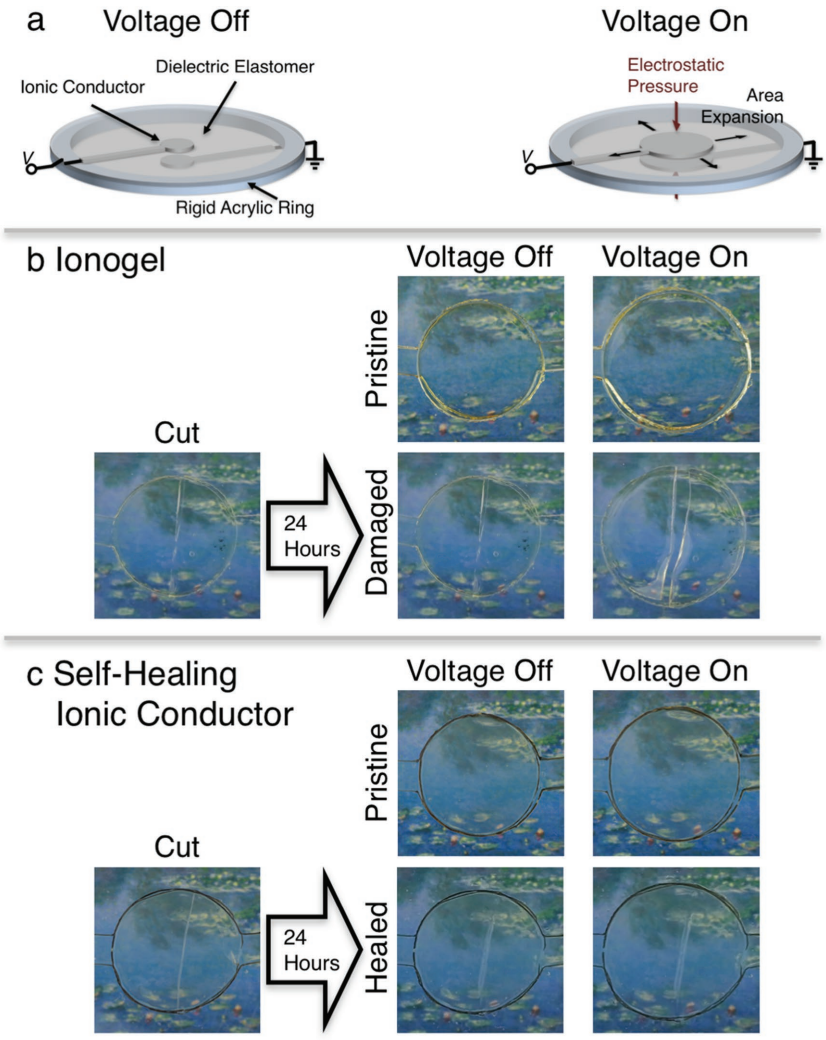

Figure 4. Comparison of the performance of two different types of stretchable, transparent, ionic conductors when used to electrically activate dielectric elastomer actuators (DEAs). a) Schematic of a DEA in the rest (voltage off) and actuated (voltage on) states. b) DEA with ionogel as stretchable conductor. Top: Pristine actuator in rest and actuated state. Bottom: A cut layer of ionic conductor did not heal over 24 h and activation of the actuator caused the cut to further open, ultimately destroying the actuator. c) DEA with the transparent, self-healing, highly stretchable ionic conductor as the stretchable conductor. Top: Pristine actuator with performance comparable to the actuator in (b). Bottom: A cut layer of ionic conductor healed over 24 h and the actuator with fully restored performance.

level of leakage of the ionic liquid, may significantly improve the lifetime of DEAs compared to DEAs that are activated with other types of ionic conductors.

In this work, we have demonstrated the first stretchable, transparent, self-healing ionic conductor using ion–dipole interactions. We anticipate that the promising approach of harnessing ion–dipole interactions will be a powerful tool in the creation of next-generation, self-healing materials. This new design of self-healing polymer opens avenues to create a family of other materials that are ionically conductive and have self-healing capabilities, enabling the synthesis of new materials with properties that can be optimized for a range of applications. Herein, we have demonstrated the benefits of using self-healing ionic conductors in soft devices, illustrated by creating soft actuators that fully recover from severe mechanical damage. We expect a large number of further applications in other areas, such as soft robotics, stretchable sensors, and energy storage.

Experimental Section

Materials: The ionic liquids BMICl, $BMIBF_4$, 1-ethyl-3-methyl imidazolium tetrafluoroborate, and EMIOTf (obtained from Sigma-Aldrich) were used as received without further purification. PVDF-*co*-HFP-5545 was purchased from 3M Co (3M Dyneon Fluoroelastomer FE). PVDF-*co*-HFP-9010 was obtained from KYNAR (Arkema Group Kynar FLEX 2801 PVDF).

Preparation of Samples: The general method for preparing various compositions, unless otherwise noted, was: 1.0 g PVDF-*co*-HFP-5545 and corresponding amounts of the ionic liquid were dissolved in 4.5 mL anhydrous acetone and stirred at room temperature for at least 4 h to give a well-dispersed solution. The solution was then poured into a petri dish. After evaporating the solvent at room temperature, the material was dried in a vacuum oven at 70 °C overnight to remove solvent residue, and then compression-molded at 70 °C into 1.0 mm thick sheets using glass slides.

The 1.0 mm thick sheets were used for testing mechanical properties and self-healing efficiency, as well as to record microscope images and for demonstration of self-healing.

Films for characterization of transmittance and ionic conductivity were prepared by pouring the solution onto a glass slide (50 mm × 75 mm) and by evaporation of the solvent at room temperature. Films for use as electrodes in dielectric elastomer actuators were prepared by pouring the solution onto a polyethylene film (50 × 75 mm) and by evaporation of the solvent at room temperature.

Preparation of Samples—Preparation of PVDF-co-HFP-9010 43 wt% EMIOTf Samples: 1.0 g PVDF-*co*-HFP-9010 and 538 µL (754 mg) EMIOTf were dissolved in 8 mL anhydrous acetone and stirred at room temperature for at least 6 h to give a well-dispersed solution. Samples for mechanical testing were obtained by pouring the solution into a 50 mL beaker and allowing the solvent to evaporate at room temperature. Films for transmittance characterization were obtained by pouring the solution into a petri dish and evaporating the solvent at room temperature. The ionogel used in experiments on dielectric elastomer actuators was prepared according to literature.[38]

Characterization of Materials: Experiments to test mechanical properties were performed using an Instron 5942. Unless otherwise noted, tensile experiments were performed at room temperature (25 °C) at a strain rate of 5 mm min^{-1} for both stretching and relaxing rate. Each mechanical test was repeated with nine individual samples of each weight fraction by preparing three different batches and each batch providing three samples. Healing experiments were performed at either room temperature or 50 °C, by gently bringing the cut pieces back into contact. The conductivity of the material was measured using a BioLogic VMP3 with samples with an area of 2.0 cm^2 and a thickness of 0.2 mm.

DSC measurements from –50 to 150 °C with a heating speed of 5 °C min^{-1} were performed using a TA Instruments Q2000. Optical micrographs were recorded with a cross-polarized optical microscope

(Leica DM2700M). FTIR data were recorded on a Nicolet 6700 FTIR. Transmission data were recorded on an Ocean Optics HR2000CG-UV-NIR spectrometer. SEM images were recorded on a FEI Nova NanoSEM 450.

Fabrication and Testing of Dielectric Elastomer Actuators: The ionic conductors were cut into circular shapes with a diameter of 17 mm with a laser cutter (Epilog Legend 36 EXT). The stretchable ionic conductors were then placed on a VHB 4910 (3M) dielectric layer which was prestretched by a factor of 3 and attached to a rigid acrylic ring. Electrically conductive carbon grease (MG Chemicals) was used to establish a connection between ionic conductors and external wires supplying high voltage. The voltage signal to power the actuators was initially generated by a Keysight Technologies 33500B signal generator and monitored with a Tektronix TBS1064 oscilloscope, and then amplified with a TREK Model 50/12 high-voltage power amplifier. To maintain constant relative humidity of the ambient air, all actuation tests with the self-healing material were performed in a custom made desiccator (Figure S16, Supporting Information), because we observed changes in the transparency of the self-healing ionic conductor as a function of humidity.

Supporting Information

Supporting Information is available from the Wiley Online Library or from the author.

Acknowledgements

Y.C. and T.G.M. contributed equally to this work. Work performed by Y.C. and C.W. was funded by startup funds from the University of California Riverside. Work performed by T.G.M., E.A., and C.K. was supported by startup funds from the University of Colorado Boulder. Work performed by S.I.A. and B.M.W. was supported by the U.S. Department of Energy, Office of Science, Early Career Research Program under Award No. DE-SC0016269.

Received: September 21, 2016
Revised: November 23, 2016
Published online:

[1] S. R. White, N. R. Sottos, P. H. Geubelle, J. S. Moore, M. R. Kessler, S. R. Sriram, E. N. Brown, S. Viswanathan, *Nature* **2001**, *409*, 794.
[2] S. D. Bergman, F. Wudl, *J. Mater. Chem.* **2008**, *18*, 41.
[3] R. P. Wool, *Soft Matter* **2008**, *4*, 400.
[4] M. Burnworth, L. Tang, J. R. Kumpfer, A. J. Duncan, F. L. Beyer, G. L. Fiore, S. J. Rowan, C. Weder, *Nature* **2011**, *472*, 334.
[5] X. Chen, M. A. Dam, K. Ono, A. Mal, H. Shen, S. R. Nutt, K. Sheran, F. Wudl, *Science* **2002**, *295*, 1698.
[6] B. Ghosh, M. W. Urban, *Science* **2009**, *323*, 1458.
[7] P. Cordier, F. Tournilhac, C. Soulié-Ziakovic, L. Leibler, *Nature* **2008**, *451*, 977.
[8] Y. Chen, A. M. Kushner, G. A. Williams, Z. Guan, *Nat. Chem.* **2012**, *4*, 467.
[9] Y. Li, L. Li, J. Sun, *Angew. Chem. Int. Ed.* **2010**, *49*, 6129.
[10] K. A. Williams, A. J. Boydston, C. W. Bielawski, *J. R. Soc. Interface* **2007**, *4*, 359.
[11] E. Palleau, S. Reece, S. C. Desai, M. E. Smith, M. D. Dickey, *Adv. Mater.* **2013**, *25*, 1589.
[12] K. K. Oehlenschlaeger, J. O. Mueller, J. Brandt, S. Hilf, A. Lederer, M. Wilhelm, R. Graf, M. L. Coote, F. G. Schmidt, C. Barner-Kowollik, *Adv. Mater.* **2014**, *26*, 3561.
[13] F. Luo, T. L. Sun, T. Nakajima, T. Kurokawa, Y. Zhao, K. Sato, A. Bin Ihsan, X. Li, H. Guo, J. P. Gong, *Adv. Mater.* **2015**, *27*, 2722.
[14] S. Ji, W. Cao, Y. Yu, H. Xu, *Adv. Mater.* **2015**, *27*, 7740.
[15] I. Jeon, J. Cui, W. R. K. Illeperuma, J. Aizenberg, J. J. Vlassak, *Adv. Mater.* **2016**, *28*, 4678.
[16] K. Liu, Y. Kang, Z. Wang, X. Zhang, *Adv. Mater.* **2013**, *25*, 5530.
[17] B. J. Blaiszik, S. L. B. Kramer, M. E. Grady, D. A. McIlroy, J. S. Moore, N. R. Sottos, S. R. White, *Adv. Mater.* **2012**, *24*, 398.
[18] Y. Li, S. Chen, M. Wu, J. Sun, *Adv. Mater.* **2012**, *24*, 4578.
[19] T.-S. Wong, S. H. Kang, S. K. Y. Tang, E. J. Smythe, B. D. Hatton, A. Grinthal, J. Aizenberg, *Nature* **2011**, *477*, 443.
[20] T. P. Huynh, H. Haick, *Adv. Mater.* **2016**, *28*, 138.
[21] Y. He, S. Liao, H. Jia, Y. Cao, Z. Wang, Y. Wang, *Adv. Mater.* **2015**, *27*, 4622.
[22] G. Cai, J. Wang, K. Qian, J. Chen, S. Li, P. S. Lee, *Adv. Sci.* **2016**, DOI: 10.1002/advs.201600190.
[23] B. C.-K. Tee, C. Wang, R. Allen, Z. Bao, *Nat. Nanotechnol.* **2012**, *7*, 825.
[24] C. Wang, H. Wu, Z. Chen, M. T. McDowell, Y. Cui, Z. Bao, *Nat. Chem.* **2013**, *5*, 1042.
[25] H. Wang, B. Zhu, W. Jiang, Y. Yang, W. R. Leow, H. Wang, X. Chen, *Adv. Mater.* **2014**, *26*, 3638.
[26] J. M. Tarascon, M. Armand, *Nature* **2001**, *414*, 359.
[27] W. H. Meyer, *Adv. Mater.* **1998**, *10*, 439.
[28] A. M. Christie, S. J. Lilley, E. Staunton, Y. G. Andreev, P. G. Bruce, *Nature* **2005**, *433*, 50.
[29] H. Wang, J. Li, F. Gong, G. Zhou, Z.-S. Wang, *J. Am. Chem. Soc.* **2013**, *135*, 12627.
[30] J. Y. Sun, C. Keplinger, G. M. Whitesides, Z. Suo, *Adv. Mater.* **2014**, *26*, 7608.
[31] C. C. Kim, H. H. Lee, K. H. Oh, J. Y. Sun, *Science* **2016**, *353*, 682.
[32] J. Lee, M. J. Panzer, Y. He, T. P. Lodge, C. D. Frisbie, *J. Am. Chem. Soc.* **2007**, *129*, 4532.
[33] J. H. Cho, J. Lee, Y. Xia, B. Kim, Y. He, M. J. Renn, T. P. Lodge, C. D. Frisbie, *Nat. Mater.* **2008**, *7*, 900.
[34] H. C. Moon, T. P. Lodge, C. D. Frisbie, *J. Am. Chem. Soc.* **2014**, *136*, 3705.
[35] Q. Zhao, A. Haines, D. Snoswell, C. Keplinger, R. Kaltseis, S. Bauer, I. Graz, R. Denk, P. Spahn, G. Hellmann, J. J. Baumberg, *Appl. Phys. Lett.* **2012**, *100*, 101902.
[36] G. Huang, Q.-P. Feng, H. Xiao, N. Li, S.-Y. Fu, *ACS Nano* **2016**, DOI: 10.1021/acsnano.6b04830.
[37] C. Keplinger, J. Y. Sun, C. C. Foo, P. Rothemund, G. M. Whitesides, Z. Suo, *Science* **2013**, *341*, 984.
[38] Y. Bai, B. Chen, F. Xiang, J. Zhou, H. Wang, Z. Suo, *Appl. Phys. Lett.* **2014**, *105*, 1.
[39] B. Chen, J. J. Lu, C. H. Yang, J. H. Yang, J. Zhou, Y. M. Chen, Z. Suo, *ACS Appl. Mater. Interfaces* **2014**, *6*, 7840.
[40] C.-H. Li, C. Wang, C. Keplinger, J.-L. Zuo, L. Jin, Y. Sun, P. Zheng, Y. Cao, F. Lissel, C. Linder, X.-Z. You, Z. Bao, *Nat. Chem.* **2016**, *8*, 618.
[41] Y. Guo, X. Zhou, Q. Tang, H. Bao, G. Wang, P. Saha, *J. Mater. Chem. A* **2016**, *4*, 8769.
[42] M. Sharma, D. Mondal, C. Mukesh, K. Prasad, *Carbohydr. Polym.* **2013**, *98*, 1025.
[43] T. J. Trivedi, D. Bhattacharjya, J.-S. Yu, A. Kumar, *ChemSusChem* **2015**, *8*, 3294.
[44] D. Mozhdehi, S. Ayala, O. R. Cromwell, Z. Guan, *J. Am. Chem. Soc.* **2014**, *136*, 16128.
[45] R. A. Fall, *MSc Thesis*, Virginia Polytechnic Institute and State University **2001**.
[46] R. K. Bose, N. Hohlbein, S. J. Garcia, A. M. Schmidt, S. van der Zwaag, *Phys. Chem. Chem. Phys.* **2015**, *17*, 1697.
[47] A. Shaaban, A. M. Schmidt, *Smart Mater. Struct.* **2016**, *25*, 84018.

[48] C.-L. Liang, Z.-H. Mai, Q. Xie, R.-Y. Bao, W. Yang, B.-H. Xie, M.-B. Yang, *J. Phys. Chem. B* **2014**, *118*, 9104.
[49] L. He, J. Sun, X. Wang, C. Wang, R. Song, Y. Hao, *Polym. Int.* **2013**, *62*, 638.
[50] C. Xing, M. Zhao, L. Zhao, J. You, X. Cao, Y. Li, *Polym. Chem.* **2013**, *4*, 5726.
[51] Y. Zhu, C. Li, B. Na, R. Lv, B. Chen, J. Zhu, *Mater. Chem. Phys.* **2014**, *144*, 194.
[52] J. Zhang, B. Sun, X. Huang, S. Chen, G. Wang, *Sci. Rep.* **2014**, *4*, 6007.
[53] H. Ye, J. Huang, J. J. Xu, A. Khalfan, S. G. Greenbaum, *J. Electrochem. Soc.* **2007**, *154*, A1048.
[54] M. A. Navarra, J. Manzi, L. Lombardo, S. Panero, B. Scrosati, *ChemSusChem* **2011**, *4*, 125.
[55] M. Joost, G. T. Kim, M. Winter, S. Passerini, *Electrochim. Acta* **2013**, *113*, 181.
[56] I. Osada, H. de Vries, B. Scrosati, S. Passerini, *Angew. Chem. Int. Ed.* **2016**, *55*, 500.
[57] C. Wang, W.-Y. Lee, D. Kong, R. Pfattner, G. Schweicher, R. Nakajima, C. Lu, J. Mei, T. H. Lee, H.-C. Wu, J. Lopez, Y. Diao, X. Gu, S. Himmelberger, W. Niu, J. R. Matthews, M. He, A. Salleo, Y. Nishi, Z. Bao, *Sci. Rep.* **2015**, *5*, 17849.
[58] M. R. Golder, B. M. Wong, R. Jasti, *Chem. Sci.* **2013**, *4*, 4285.
[59] J.-D. Chai, M. Head-Gordon, *J. Chem. Phys.* **2008**, *128*, 84106.
[60] J. Le Bideau, L. Viau, A. Vioux, *Chem. Soc. Rev.* **2011**, *40*, 907.
[61] R. P. Sijbesma, F. H. Beijer, L. Brunsveld, B. J. B. Folmer, J. H. K. K. Hirschberg, R. F. M. Lange, J. K. L. Lowe, E. W. Meijer, *Science* **1997**, *278*, 1601.
[62] R. C. Agrawal, G. P. Pandey, *J. Phys. D: Appl. Phys.* **2008**, *41*, 223001.
[63] Z. Li, G. Su, D. Gao, X. Wang, X. Li, *Electrochim. Acta* **2004**, *49*, 4633.
[64] S. Bauer, S. Bauer-Gogonea, I. Graz, M. Kaltenbrunner, C. Keplinger, R. Schwödiauer, *Adv. Mater.* **2014**, *26*, 149.
[65] R. F. Shepherd, F. Ilievski, W. Choi, S. A. Morin, A. A. Stokes, A. D. Mazzeo, X. Chen, M. Wang, G. M. Whitesides, *Proc. Natl. Acad. Sci. USA* **2011**, *108*, 20400.
[66] S. A. Morin, R. F. Shepherd, S. W. Kwok, A. A. Stokes, A. Nemiroski, G. M. Whitesides, *Science* **2012**, *337*, 828.
[67] I. A. Anderson, T. A. Gisby, T. G. McKay, B. M. O'Brien, E. P. Calius, *J. Appl. Phys.* **2012**, *112*, 41101.
[68] R. Pelrine, R. Kornbluh, Q. Pei, J. Joseph, *Science* **2000**, *287*, 836.
[69] S. Rosset, H. R. Shea, *Appl. Phys. A* **2013**, *110*, 281.